Available online at www.sciencedirect.com
ScienceDirect
International Journal of Solids and Structures 45 (2008) 3751–3768
INTERNATIONAL JOURNAL OF SOLIDS AND STRUCTURES
www.elsevier.com/locate/ijsolstr

Mechanical properties of two novel planar lattice structures

Y.H. Zhang, X.M. Qiu, D.N. Fang *

Department of Engineering Mechanics, Tsinghua University, Beijing 100084, PR China

Received 15 April 2007; received in revised form 28 September 2007
Available online 22 October 2007

Abstract

Two novel statically indeterminate planar lattice materials are designed: a new Kagome cell (N-Kagome) and a statically indeterminate square cell (SI-square). Their in-plane mechanical properties, such as stiffness, yielding, buckling and collapse mechanisms are investigated by analytical methods. The analytical stiffness is also verified by means of finite element (FE) simulations. In the case of uniaxial loading, effective modulus, yield strength, buckling strength and critical relative density are compared for various lattice structures. At a critical relative density, the collapse mode will change from buckling to yielding. Elastic buckling under macroscopic shear loading is found to have significant influence on failure of lattice structures, especially at low relative densities. Comparison of the analytical bulk and shear moduli with the Hashin–Shtrikman bounds indicates that the mechanical properties of the SI-square honeycomb are relatively close to being optimal. It is found that compared with the other existing stretching-dominated 2D lattice structures, the N-Kagome cell possesses the largest continuous cavities for fixed relative densities and wall thicknesses, which is convenient for oil storage, disposal of heat exchanger, battery deploying and for other functions. And the initial yield strength of the N-Kagome cell is slightly lower than that of the Kagome cell. The SI-square cell has similar high stiffness and strength as the mixed cell while its buckling resistance is about twice than that of the mixed cell.

Keywords: Planar lattice structures; Kagome; Mechanical properties; Collapse

1. Introduction

In order to increase the efficiency of structure, reducing weight and enforcing load carrying capacity are always the primary demand in design, especially for structures in aircraft and satellite. Recently, lightweight structures including metal foams, honeycomb sandwiches and lattice structures have been popularly used in engineering applications (Gibson and Ashby, 1997; Ashby et al., 2000; Smith et al., 2001), for their superior properties of high relative stiffness and strength, energy absorbability and heat insulation.

Lattice structure is a kind of periodic trusses patterned like moleculelattice. Usually there is no filling in the space between frames of those 2D or 3D constructions. Because of large value of interspace, sufficient quantity of mass could be reduced. Hence the relative stiffness and relative strength are increased. With the same mate-

* Corresponding author. Tel.: +86 10 62772923; fax: +86 10 62781824.
E-mail address: fangdn@mail.tsinghua.edu.cn (D.N. Fang).

0020-7683/$ - see front matter © 2007 Elsevier Ltd. All rights reserved.
doi:10.1016/j.ijsolstr.2007.10.005

rial and weight, repetitive lattice is stiffer and stronger than metal foam (Evans et al., 2001; Evans, 2001). Beside load carrying ability, the interspace in the frame constructions could be used for oil storage, battery deploying and other functions. The prismatic cellular structure could also be used in convectional heat exchanging (Ashby, 2000; Kim et al., 2004, 2005). Furthermore, repetitive truss has the potential application in actuation and damped vibrations (Lu et al., 2005). The multifunctional characters provide lattice material various usage in optimization design (Liu and Lu, 2004; Wicks and Hutchinson, 2001).

As a kind of lattice material, hexagonal honeycomb which has very low relative densities and elastic buckling strength was proverbially focused. Gibson and Ashby (1997) presented basic results about ideal and commercial hexagonal lattice. The initial plastic collapse and subsequent post-buckling of hexagonal aluminum cell were analyzed by Papka and Kyriakides (1998), and both experiments and finite element analysis under in-plane loading conditions were performed in their paper. Onck et al. (2001) and Andrews et al. (2001) investigated the specimen size effects of hexagonal honeycomb. Elastic buckling of the hexagonal honeycomb was studied by Gibson and Ashby (1997) and Zhang and Ashby (1992). Wang and McDowell (2003) analyzed the imperfection influence for three kinds of honeycombs.

The in-plane mechanical performances of the bending-dominated cell structures, such as the hexagonal honeycomb are inferior to that of the stretching-dominated structures, such as the triangular and Kagome cells, especially at low relative densities. However, cells with slightly complicated patterns did not gain any attentions for their manufacturing difficulties. Recently, a new kind of fabrication method named *powder processing technology* has been developed by Lightweight Structures Group at Georgia Tech (Cochran et al., 2000), and various kinds of complicated cells could be made by this approach. A ceramic paste is extruded through a die, dried, and then reduced in a hydrogen atmosphere, resulting in metallic honeycomb structures. Wang and McDowell (2004, 2005) systematically calculated the stiffness and strength of seven different types of cell patterns in both the principal directions and diagonal directions. Yield surfaces were also compared for different honeycomb structures in their paper. Hutchinson et al. (2003) analyzed the collapse mode of the Kagome cell.

Recently, planar lattice structures with complicated cells have been focused on for different kinds of applications, especially stretching-dominated cells, including statically determinate cells and statically indeterminate cells. Note that the study on mechanical properties of statically indeterminate cells is still scarce. Wang and McDowell (2004) calculated the stiffness and initial yield strength of the mixed cell in the principal directions and diagonal directions. But the results of both collapse mode and yield surface of statically indeterminate cells have not been reported so far. Besides, very limited statically indeterminate cells have been considered in previous investigations.

In this paper, two novel statically indeterminate lattice structures are designed and their mechanical behaviors are analyzed. First in Section 2, the design of these two structures is introduced. Then the in-plane effective moduli of these two structures are analyzed, verified by FE simulations and also compared with the corresponding Hashin–Shtrikman bounds in Sections 3 and 4. In Section 5, the yield surface and buckling surface are calculated and the collapse mechanisms are analyzed. Finally in Section 6, the effective mechanical properties of various lattice structures are compared under uniaxial loading conditions.

2. Design of two novel planar lattice structures

The work of Wang and McDowell (2004, 2005) indicates that the stiffness and yield surface of the Kagome cell are all the same as those of the fully triangulated cell, while the buckling strength of the Kagome cell is four times that of the fully triangulated cell. In order to illustrate this result, the resemblance of the configuration between these two cells is analyzed. As shown in Fig. 1, the fully triangulated cell and the Kagome cell are both composed of three groups of lines. The first two groups of lines (solid line) are exactly the same, and only the third group lines (dash line) are different. The third group lines cross the intersections of the first two groups of lines for the triangular cell, while they cross the midpoints between the intersections for the Kagome cell. With the same relative density and wall thickness, the strut length of the Kagome cell is only half that of the triangular cell, thus the buckling strength of the Kagome cell is four times that of the triangular cell.

As shown in Fig. 1c, the configuration of the mixed cell (Wang and McDowell, 2004), composed of four groups of lines, is similar to that of the fully triangulated cell. The first two groups of lines are horizontal

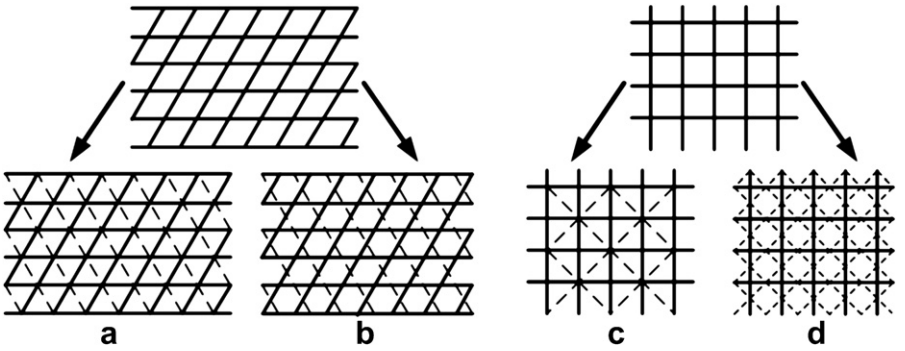

Fig. 1. The configurations of the (a) triangular, (b) Kagome, (c) mixed and (d) SI-square cells.

and vertical, respectively, and the last two groups of lines cross the intersections of the first two groups of lines. According to the fact that the Kagome cell possesses higher buckling strength than the triangular cell, a novel statically indeterminate square (*SI-square*) cell as shown in Fig. 1d is designed through making the last two groups of lines cross the midpoints between the intersections of the first two groups of lines. The calculations given in Section 6 indicate that the buckling strength of this SI-square cell is about twice that of the mixed cell. Besides, the utmost yield strength of the SI-square cell is calculated and found to be higher than the initial yield strength of the Kagome cell. Therefore, the SI-square honeycomb is an excellent structure in load carrying.

The configuration of the SI-square cell can also be considered as the 2D degeneration from the 3D pyramid lattice structure. A representative unit cell as sketched in Fig. 3a is employed for analyzing mechanical properties. The relative density of this cell is,

$$r = \frac{\rho^*}{\rho_s} = \left(2 + \sqrt{2}\right)\frac{t}{l}, \tag{1}$$

where r is relative density, l wall length and t in-plane wall thickness. ρ^* and ρ_s are densities of the cell and the solid material, respectively. The out-of-plane dimension of the honeycomb is noted as b.

Analogously, a new Kagome cell as shown in Fig. 2 can be also designed, which is called *N-Kagome* in this paper. According to the analytical results in Section 6, for fixed relative densities and wall thicknesses, the N-Kagome cell has larger continuous cavities than the other existing stretching-dominated 2D lattice structures (triangular, Kagome, diamond, mixed and SI-square cells), while the yield strength of the N-Kagome cell is slightly lower than that of the Kagome cell. Therefore, the N-Kagome lattice structure is convenient for oil storage, disposal of heat exchanger, battery deploying and for other functions, This honeycomb configuration is the 2D structure degenerated from the 3D Kagome lattice structure. The representative unit cell shown in Fig. 4a is adopted in our analysis. Compared with the Kagome cell, the N-Kagome cell has three short struts inside the triangle and its relative density is

$$r = \frac{\rho^*}{\rho_s} = \left(\sqrt{3} + 1\right)\frac{t}{l}, \tag{2}$$

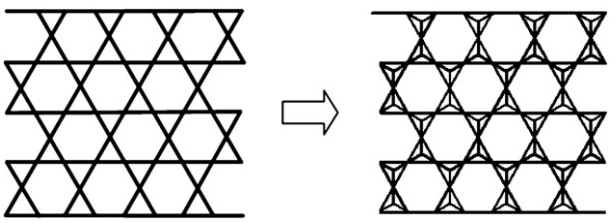

Fig. 2. The configurations of (a) the Kagome cell and (b) the N-Kagome cell.

where l is the length of long struts. t and b are in-plane and out-of-plane thicknesses of the cell wall, respectively.

3. In-plane effective moduli in the principal directions

For honeycomb structures under different kinds of in-plane loadings, three types of stress may exist inside the cell walls: bending, tension or shear stress. The lattices dominantly subjected to tensional or compressive stress are called *stretching-dominated structures*. As shown in Fig. 1, all of four lattice patterns, including the triangular, Kagome, mixed and SI-square, belong to stretching-dominated honeycombs. In the present analysis, the material of cell walls is assumed to be perfectly elastic–plastic. Since the SI-square and N-Kagome cells are both statically indeterminate structures, they may sustain residual stresses without any applied loads. These parts of stresses are neglected in the analysis. Timoshenko's beam and column theories (Timoshenko and Gere, 1961; Gere and Timoshenko, 1984) are adopted, and each cell wall is simplified as a truss subjected to only axial force.

3.1. Effective moduli of the SI-square cell

As shown in Fig. 3c, under loading of a axial stress, σ_1, in the x_1 direction, the internal forces of each strut in the unit cell of the SI-square lattice structure are solved. Noting that the two struts in the same direction have same internal forces, only four internal forces are considered. Let N_i be the internal force of ith strut, $i = 1\ldots4$, and the mark of each strut is shown in Fig. 3a. By employing the energy method, the internal forces of each strut can be obtained, i.e.

$$N_1 = N_4 = \frac{2-\sqrt{2}}{2}\sigma_1 bl, \quad N_2 = -\left(\sqrt{2}-1\right)\sigma_1 bl, \quad N_3 = \sigma_1 bl. \tag{3}$$

Thus, the equivalent strains in the x_1 and x_2 directions of the unit cell, ε_1 and ε_2, are

$$\varepsilon_1 = \frac{N_3}{E_s A}, \quad \varepsilon_2 = \frac{N_2}{E_s A}, \tag{4}$$

where E_s is Young's modulus of the solid material and $A = bt$ is the truss section area. From Eqs. (3) and (4), the effective modulus in the x_1 direction and Poisson ratio, E_1^* and v_{12}^*, can be calculated as following,

$$\frac{E_1^*}{E_s} = 0.293r, \quad v_{12}^* = -\frac{\varepsilon_2}{\varepsilon_1} = 0.414. \tag{5}$$

Because of symmetry, the effective modulus in the x_2 direction, E_2^*, is the same as that in the x_1 direction, i.e. $E_2^*/E_s = E_1^*/E_s = 0.293r$.

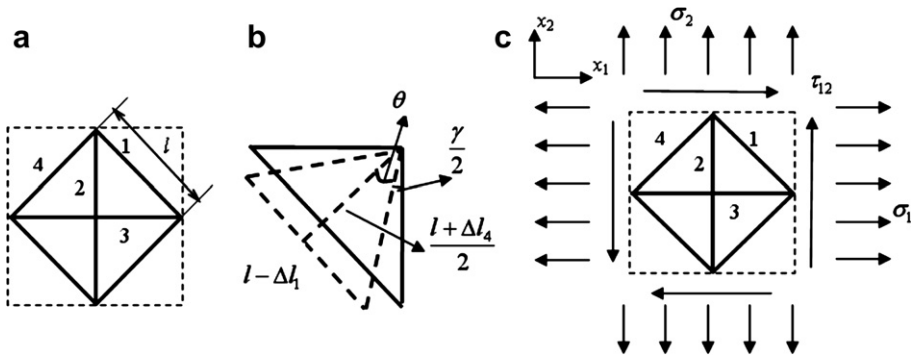

Fig. 3. (a) The unit cell of the SI-square lattice structure, (b) the deformation profile of the unit cell under loading of a shear stress, τ_{12}, and (c) the unit cell under a combined in-plane stress state.

With the unit cell under shear stress in the principal direction, the internal force and deformation are determined by the symmetrical and antisymmetrical conditions, i.e.

$$N_1 = -\tau_{12} bl, \quad N_4 = \tau_{12} bl, \quad \Delta l_1 = \frac{\tau_{12} bl^2}{E_s A} \quad \text{(compression)}, \quad \Delta l_4 = \frac{\tau_{12} bl^2}{E_s A} \quad \text{(tension)}, \tag{6}$$

where Δl_1 and Δl_4 are the deformations of 1st and 4th struts, respectively.

Considering the deformation profile shown in Fig. 3b, in the range of infinitesimal deformation the shear strain, γ, can be obtained as follow,

$$\gamma \approx 2 \tan \frac{\gamma}{2} = 2 \frac{1 - \tan \theta}{1 + \tan \theta}, \tag{7}$$

where θ is the angle between the horizontal strut and inclined strut after deformation, and $\tan \theta = \frac{l - \Delta l_1}{l + \Delta l_4}$. From Eqs. (6) and (7), one can easily get the shear modulus, G_{12}^*, i.e.

$$\frac{G_{12}^*}{E_s} = 0.146 r. \tag{8}$$

3.2. Effective moduli of the N-Kagome cell

As shown in Fig. 4b, consider a case that the unit cell of the N-Kagome lattice structure is under loading of a axial stress, σ_1, in the x_1 direction. By exploiting the energy method, the internal force in each strut and the strains in the x_1 and x_2 directions are calculated as follows,

$$\begin{aligned} &N_1 = N_2 = -\frac{3 - \sqrt{3}}{6} \sigma_1 bl, \quad N_3 = \frac{7\sqrt{3} - 3}{6} \sigma_1 bl, \quad N_4 = N_5 = N_6 = \frac{\sqrt{3} - 1}{2} \sigma_1 bl, \\ &\varepsilon_1 = \frac{2 + 3\sqrt{3}}{3 + \sqrt{3}} \frac{\sigma_1 l}{E_s t}, \quad \varepsilon_2 = \frac{2 + \sqrt{3}}{3 + \sqrt{3}} \frac{\sigma_1 l}{E_s t}, \end{aligned} \tag{9}$$

where N_i denotes the internal force of ith strut, $i = 1 \ldots 6$, and the mark of each strut is shown in Fig. 4a. Thus the effective modulus in the x_1 direction and Poisson ratio can be obtained,

$$\frac{E_1^*}{E_s} = 0.241 r, \quad v_{12}^* = \frac{5 + 4\sqrt{3}}{23} = 0.519. \tag{10}$$

Similarly, we can also have the solutions of the unit cell under uniaxial compression in the x_2 direction and under shear. The effective modulus in the x_2 direction and the shear modulus are,

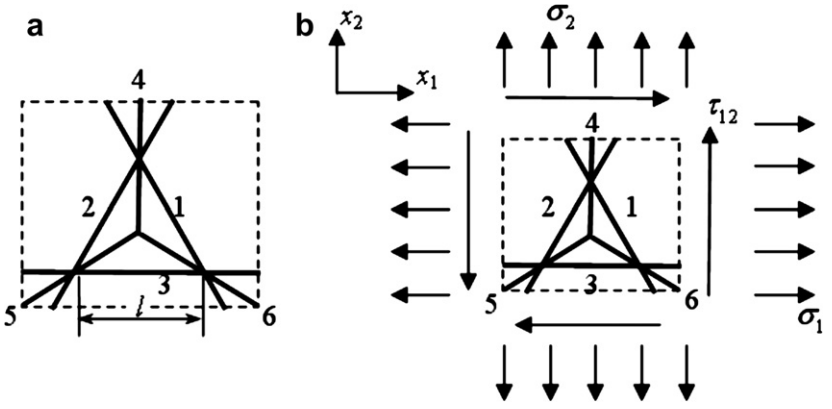

Fig. 4. (a) The unit cell of the N-Kagome lattice structure and (b) the unit cell under a combined in-plane stress state.

$$\frac{E_2^*}{E_s} = 0.241r, \quad \frac{G_{12}^*}{E_s} = 0.0793r. \tag{11}$$

It is clear that this N-Kagome cell is also transversely isotropic and the same as the Kagome cell.

3.3. Verification of FE simulations

Two-dimensional FE calculations are performed by use of the commercial software ABAQUS to validate the analytical stiffness results. In the theoretical analysis, the struts are all assumed to be pin-jointed, while in the FE simulations the struts are all rigid jointed. The effective elastic moduli of the above two unit cells shown in Figs. 3a and 4a are calculated. Beam elements (B32 in ABAQUS denotion) and very fine meshes are adopted to ensure accuracy. The periodic boundary conditions adopted in our FE calculations are as follows: the unit cell faces are constrained to be flat, parallel and mutually perpendicular. In the ABAQUS software there is a function to complete the periodic boundary conditions. For the tensional modulus, the normal stress is loaded and the effective strain is obtained. For the shear modulus, the shear mode is imposed and then the resultant stress is calculated. The relative density is changed by varying the wall thickness t for a fixed strut length l. The beam section is assumed to be rectangular and the material properties are $E_s = 100$ GPa and $v_s = 0.33$.

Fig. 5 shows that the elastic modulus is linearly dependent on the relative density of the cell. It can be seen that the analytical results are in good agreement with the FE data points. Considering that the joint assumptions are different in the analytical theory and FE calculations, these two cell configurations are confirmed to be stretching-dominated structures. In the case of infinitesimal deformation, the pin-jointed assumption used here has sufficient accuracy in the analysis of stiffness.

4. Comparison of elastic properties with the Hashin–Shtrikman bounds

The well-known Hashin–Shtrikman bounds can provide the best possible bounds on the effective elastic moduli and conductivity of isotropic two-phase composites for a given phase volume fraction (Hashin and Shtrikman, 1963; Hashin, 1965). Generalization of the Hashin–Shtrikman bounds has been performed to be applicable for macroscopically anisotropic composites by several investigators (Kantor and Bergman, 1984; Francfort and Murat, 1986; Milton and Kohn, 1988). In this section, the concise form of Hashin–Shtrikman bounds generalized by Milton and Kohn (1988) is adopted to bound the bulk and shear moduli of the two-dimensional macroscopically isotropic N-Kagome cell and anisotropic SI-square cell. Note that for cellular materials, the lower bound is a constant (Milton and Kohn, 1988; Hyun and Torquato, 2000), so only the upper bound can be discussed.

For the two-dimensional macroscopically isotropic N-Kagome cell, the linear constitutive relations can be written as

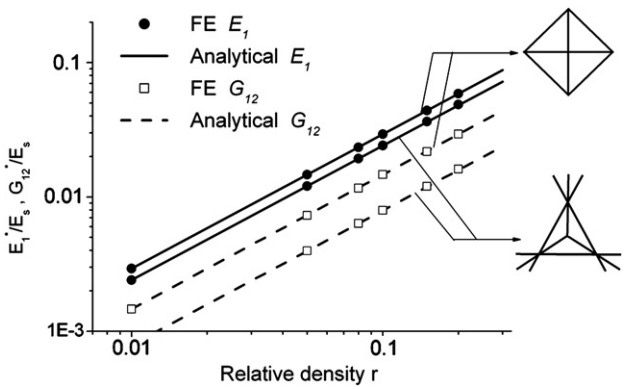

Fig. 5. The elastic moduli of the SI-square cell and the N-Kagome cell.

$$\sigma_{\alpha\beta} = k^* \varepsilon_{\gamma\gamma} \delta_{\alpha\beta} + 2G^* \varepsilon_{\alpha\beta}, \tag{12}$$

where k^* and G^* are the effective bulk and shear moduli of the lattice material. $\sigma_{\alpha\beta}$ and $\varepsilon_{\alpha\beta}$ are stress and strain components, $\alpha, \beta = 1,2$. $\delta_{\alpha\beta}$ is the Kronecker delta. Let k_s and G_s be the bulk and shear modulus of the solid material, respectively. Noting that the volume fraction of the solid material is just equal to the relative density, r, the Hashin–Shtrikman upper bounds on the effective moduli of the N-Kagome cell can be given by

$$\frac{k^*}{k_s} \leqslant \frac{1 - v_s}{2 - r - v_s r} r, \quad \frac{G^*}{G_s} \leqslant \frac{1 + v_s}{4 - 3r + v_s r} r. \tag{13}$$

It should be explained that these two bounds (Eq. (13)) have no difference with those of the other macroscopically isotropic cellular solid.

For the two-dimensional macroscopically anisotropic SI-square cell, the square symmetry dictates that the linear constitutive relation can be written as

$$\sigma_{11} = (k^* + G_p^*)\varepsilon_{11} + (k^* - G_p^*)\varepsilon_{22}, \quad \sigma_{22} = (k^* - G_p^*)\varepsilon_{11} + (k^* + G_p^*)\varepsilon_{22}, \quad \sigma_{12} = 2G_{12}^* \varepsilon_{12}, \tag{14}$$

where G_p^* is a quantity that equals to $E_1^*/2(1 + v_{12}^*)$. The generalized Hashin–Shtrikman upper bounds on the effective moduli of the SI-square cell are given by

$$\frac{k^*}{k_s} \leqslant \frac{1 - v_s}{2 - r - v_s r} r, \quad G_e = \frac{1}{1 - \frac{G_{12}^*}{G_s}} + \frac{1}{1 - \frac{G_p^*}{G_s}} \leqslant 2 + \frac{1 + v_s}{2} \frac{r}{1 - r}, \tag{15}$$

where G_e is simply a symbol for a combination of shear modulus, and the explicit bounds for only G_{12}^*/G_s or only G_p/G_s cannot be obtained from this generalized bounds. The lower bounds are 2 for G_e and zero for k^* of the SI-square cell, and zero for k^* and $G^*$of the N-Kagome cell.

In the low-density limit ($r \to 0$), these four bounds (Eqs. (13) and (15)) become

$$\frac{k^*}{k_s} \leqslant \frac{1 - v_s}{2} r, \quad \frac{G^*}{G_s} \leqslant \frac{1 + v_s}{4} r \text{ (for the N-Kagome cell)}, \tag{16}$$

$$\frac{k^*}{k_s} \leqslant \frac{1 - v_s}{2} r, \quad G_e = \frac{1}{1 - \frac{G_{12}^*}{G_s}} + \frac{1}{1 - \frac{G_p^*}{G_s}} \leqslant 2 + \frac{1 + v_s}{2} r \text{ (for the SI-square cell)}. \tag{17}$$

In Section 3, the analytical results related to the modulus and Poisson ratio already are given. Thus, analytical results of the bulk modulus and the shear modulus of these two cells can be obtained as follows:

$$\frac{k^*}{k_s} = \frac{1 - v_s}{2} r, \quad \frac{G^*}{G_s} = 0.159(1 + v_s) r \text{ (for the N-Kagome cell)}, \tag{18}$$

$$\frac{k^*}{k_s} = \frac{1 - v_s}{2} r, \quad G_e = \frac{1}{1 - \frac{G_{12}^*}{G_s}} + \frac{1}{1 - \frac{G_p^*}{G_s}} = 2 + \frac{\frac{2-\sqrt{2}}{2}(1 + v_s) r}{1 - \frac{2-\sqrt{2}}{2}(1 + v_s) r} + \frac{\frac{\sqrt{2}-1}{2}(1 + v_s) r}{1 - \frac{\sqrt{2}-1}{2}(1 + v_s) r} \text{ (for the SI-square cell)}. \tag{19}$$

A comparison of the analytical bulk and shear moduli and the corresponding Hashin–Shtrikman upper bounds for these two cells are demonstrated in Fig. 6. It can be seen from Fig. 6a that the analytical results for both the bulk modulus, k^*, and the combination of shear modulus, G_e, of the SI-square cell are approximately the same as those of the Hashin–Shtrikman upper bound at low relative densities ($r < 0.1$). The relatively slight reduction of the analytical results at high relative densities ($r > 0.1$) is mainly due to the excessive estimates of relative densities by the linear relation with t/l. Thus it can be considered that the SI-square lattice attains the Hashin–Shtrikman upper bounds on both the bulk and shear moduli approximately. However, the N-Kagome lattice only achieves the bulk modulus upper bound. The reason why the shear modulus upper bound is not achieved for the N-Kagome lattice is that the short struts within the triangles do not bear any load when the unit cell is under shear loading. Therefore, it is indicated that both the values of the bulk

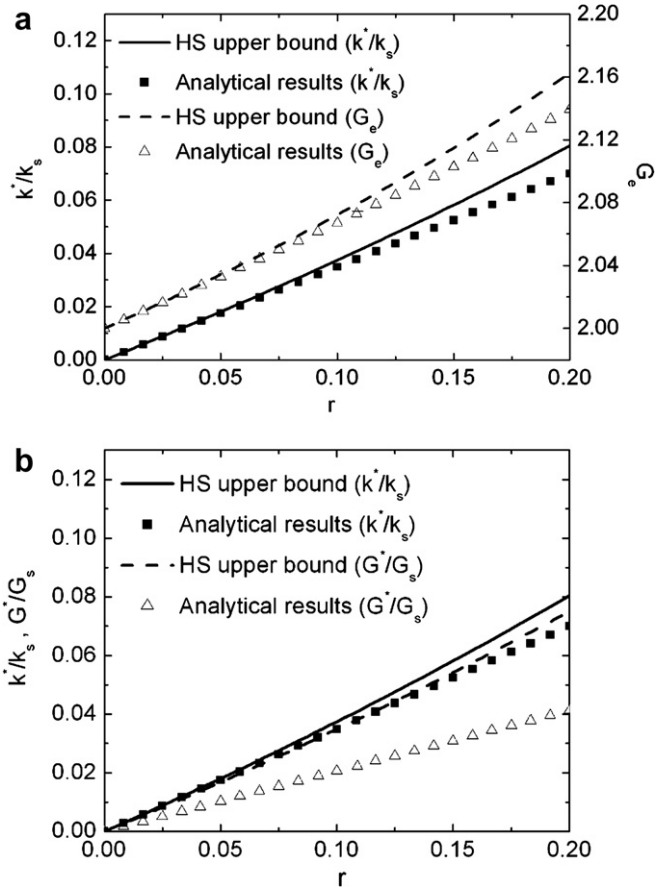

Fig. 6. Effective bulk and shear moduli of (a) the SI-square cell and (b) the N-Kagome cell versus the relative densities ($v_s = 0.3$).

modulus, k^*, and the combination of shear modulus, G_e, are relatively close to being optimal for the SI-square honeycomb.

5. Yield surface, buckling surface and collapse analysis

For applications of the SI-square and N-Kagome cells, the yield and buckling surface equations of both the two cells are calculated, and the collapse analyses are also performed in this section.

5.1. Yield surface

Consider a case that the unit cells of both the SI-square and N-Kagome lattices are subjected to the in-plane axial stresses σ_1 and σ_2 in two orthogonal directions, and shear stress, τ_{12}, as shown in Figs. 3c and 4b. The internal forces within each strut are calculated by superposition of biaxial tension and shear for both the two cells, which are given by

$$\begin{aligned} &N_1 = \tfrac{2-\sqrt{2}}{2}(\sigma_1+\sigma_2)bl - \tau_{12}bl, \quad N_2 = -\left(\sqrt{2}-1\right)\sigma_1 bl + \sigma_2 bl \\ &N_3 = \sigma_1 bl - \left(\sqrt{2}-1\right)\sigma_2 bl, \quad N_4 = \tfrac{2-\sqrt{2}}{2}(\sigma_1+\sigma_2)bl + \tau_{12}bl \end{aligned} \quad \text{(SI-square)}, \tag{20}$$

$$\begin{aligned} &N_1 = bl\left(-\tfrac{3-\sqrt{3}}{6}\sigma_1 + \tfrac{5\sqrt{3}-3}{6}\sigma_2 - 2\tau_{12}\right), \quad N_2 = bl\left(-\tfrac{3-\sqrt{3}}{6}\sigma_1 + \tfrac{5\sqrt{3}-3}{6}\sigma_2 + 2\tau_{12}\right) \\ &N_3 = bl\left(\tfrac{7\sqrt{3}-3}{6}\sigma_1 - \tfrac{3+\sqrt{3}}{6}\sigma_2\right), \quad N_4 = N_5 = N_6 = \tfrac{\sqrt{3}-1}{2}(\sigma_1+\sigma_2)bl \end{aligned} \quad \text{(N-Kagome)}. \tag{21}$$

If $N_i = \sigma_{ys} bt$, $i = 1\ldots4$, the struts yield. The initial yielding occurs in the unit cell when any strut in the unit cell yields. Therefore, the initial yield equation of the SI-square cell or N-Kagome cell honeycomb is given by

$$\max\left(\frac{|N_i|}{bt\sigma_{ys}} - 1\right) = 0, \quad i = 1\ldots4. \tag{22}$$

The full expressions of normalized initial yield surface equations for the two cells are obtained by substituting Eqs. (20) and (21) into Eq. (22), i.e.

$$\max\left\{\begin{array}{l}\left(\left|\left(\frac{\sigma_1}{r\sigma_{ys}}+\frac{\sigma_2}{r\sigma_{ys}}\right)-\left(2+\sqrt{2}\right)\frac{\tau_{12}}{r\sigma_{ys}}\right|-1\right),\left(\left|-\sqrt{2}\frac{\sigma_1}{r\sigma_{ys}}+\left(2+\sqrt{2}\right)\frac{\sigma_2}{r\sigma_{ys}}\right|-1\right),\\ \left(\left|\left(\frac{\sigma_1}{r\sigma_{ys}}+\frac{\sigma_2}{r\sigma_{ys}}\right)+\left(2+\sqrt{2}\right)\frac{\tau_{12}}{r\sigma_{ys}}\right|-1\right),\left(\left|\left(2+\sqrt{2}\right)\frac{\sigma_1}{r\sigma_{ys}}-\sqrt{2}\frac{\sigma_2}{r\sigma_{ys}}\right|-1\right)\end{array}\right\} = 0 \quad \text{(SI-square)}, \tag{23}$$

$$\max\left\{\begin{array}{l}\left|-\frac{\sqrt{3}}{3}\frac{\sigma_1}{r\sigma_{ys}}+\frac{6+\sqrt{3}}{3}\frac{\sigma_2}{r\sigma_{ys}}-2\left(1+\sqrt{3}\right)\frac{\tau_{12}}{r\sigma_{ys}}\right|-1,\\ \left|-\frac{\sqrt{3}}{3}\frac{\sigma_1}{r\sigma_{ys}}+\frac{6+\sqrt{3}}{3}\frac{\sigma_2}{r\sigma_{ys}}+2\left(1+\sqrt{3}\right)\frac{\tau_{12}}{r\sigma_{ys}}\right|-1,\\ \left|\frac{9+2\sqrt{3}}{3}\frac{\sigma_1}{r\sigma_{ys}}-\frac{3+2\sqrt{3}}{3}\frac{\sigma_2}{r\sigma_{ys}}\right|-1\end{array}\right\} = 0 \quad \text{(N-Kagome)}. \tag{24}$$

Here, it should be explained that for the N-Kagome cell, the value of $|N_4|$ is never maximal among $|N_i|$, $i = 1\ldots4$, which means the three short struts inside the triangle (the 4th, 5th and 6th struts) will never yield earlier than other struts under any applied stresses. Therefore, the yield surface equation of the N-Kagome cell can be simplified as the form of Eq. (24).

Beside the above yield surfaces for in-plane stress state, the yield surface for triaxial loading could also be obtained using the method employed by Wang and McDowell (2005). Here, only the yield surfaces of the triaxial tension or triaxial compression conditions are analyzed. The unit cell is subjected to triaxial normal stresses, σ_1, σ_2 and σ_3, along the x_1, x_2 and x_3 directions, respectively. The corresponding initial yield surface equations are given as follows

$$\max\left\{\begin{array}{l}\left(\left|\left(\frac{\sigma_1}{r\sigma_{ys}}+\frac{\sigma_2}{r\sigma_{ys}}\right)^2-\left(\frac{\sigma_1}{r\sigma_{ys}}+\frac{\sigma_2}{r\sigma_{ys}}\right)\frac{\sigma_3}{r\sigma_{ys}}+\left(\frac{\sigma_3}{r\sigma_{ys}}\right)^2\right|-1\right),\\ \left(\left|\left[\sqrt{2}\frac{\sigma_1}{r\sigma_{ys}}-\left(2+\sqrt{2}\right)\frac{\sigma_2}{r\sigma_{ys}}\right]^2+\left[\sqrt{2}\frac{\sigma_1}{r\sigma_{ys}}-\left(2+\sqrt{2}\right)\frac{\sigma_2}{r\sigma_{ys}}\right]\frac{\sigma_3}{r\sigma_{ys}}+\left(\frac{\sigma_3}{r\sigma_{ys}}\right)^2\right|-1\right),\\ \left(\left|\left[\left(2+\sqrt{2}\right)\frac{\sigma_1}{r\sigma_{ys}}-\sqrt{2}\frac{\sigma_2}{r\sigma_{ys}}\right]^2-\left[\left(2+\sqrt{2}\right)\frac{\sigma_1}{r\sigma_{ys}}-\sqrt{2}\frac{\sigma_2}{r\sigma_{ys}}\right]\frac{\sigma_3}{r\sigma_{ys}}+\left(\frac{\sigma_3}{r\sigma_{ys}}\right)^2\right|-1\right)\end{array}\right\} = 0 \text{ (SI-square)}, \tag{25}$$

$$\max\left\{\begin{array}{l}\left(\left|\left(\frac{\sqrt{3}}{3}\frac{\sigma_1}{r\sigma_{ys}}-\frac{6+\sqrt{3}}{3}\frac{\sigma_2}{r\sigma_{ys}}\right)^2+\left(\frac{\sqrt{3}}{3}\frac{\sigma_1}{r\sigma_{ys}}-\frac{6+\sqrt{3}}{3}\frac{\sigma_2}{r\sigma_{ys}}\right)\frac{\sigma_3}{r\sigma_{ys}}+\left(\frac{\sigma_3}{r\sigma_{ys}}\right)^2\right|-1\right),\\ \left(\left|\begin{array}{l}\left(\frac{9+2\sqrt{3}}{3}\frac{\sigma_1}{r\sigma_{ys}}-\frac{3+2\sqrt{3}}{3}\frac{\sigma_2}{r\sigma_{ys}}\right)^2\\ -\left(\frac{9+2\sqrt{3}}{3}\frac{\sigma_1}{r\sigma_{ys}}-\frac{3+2\sqrt{3}}{3}\frac{\sigma_2}{r\sigma_{ys}}\right)\frac{\sigma_3}{r\sigma_{ys}}+\left(\frac{\sigma_3}{r\sigma_{ys}}\right)^2\end{array}\right|-1\right)\end{array}\right\} = 0 \text{ (N-Kagome)}. \tag{26}$$

The analytical yield surfaces of the SI-square cell and the N-Kagome cell are shown in Fig. 7, in the space of normalized stress. Both the two initial yield surfaces are closed, convex and anisotropic. Due to the dominance of cell wall stretching, the yield surfaces consist of only planar facets. The initial yield surface equation of the mixed cell is calculated by use of the same method. It has the same shape as that of the SI-square cell, and the difference only exists in surface directions. If one of the cells is rotated an angle of $\pi/4$, the two initial yield surfaces will be exactly the same.

It is noted that the initial yield surface of the N-Kagome is slightly smaller than that of the Kagome cell (Wang and McDowell, 2005). But in the condition of the same relative density and wall thickness, the N-Kagome cell can provide more usable interspace, especially for the situation of plane strain state, which can be employed for oil storage, disposal of heat exchanger, battery deploying and for other functions. At the expense of slight decrease of the loading carrying ability of the Kagome lattice, the N-Kagome lattice has potential application in multifunction designs, especially when a large interspace is needed.

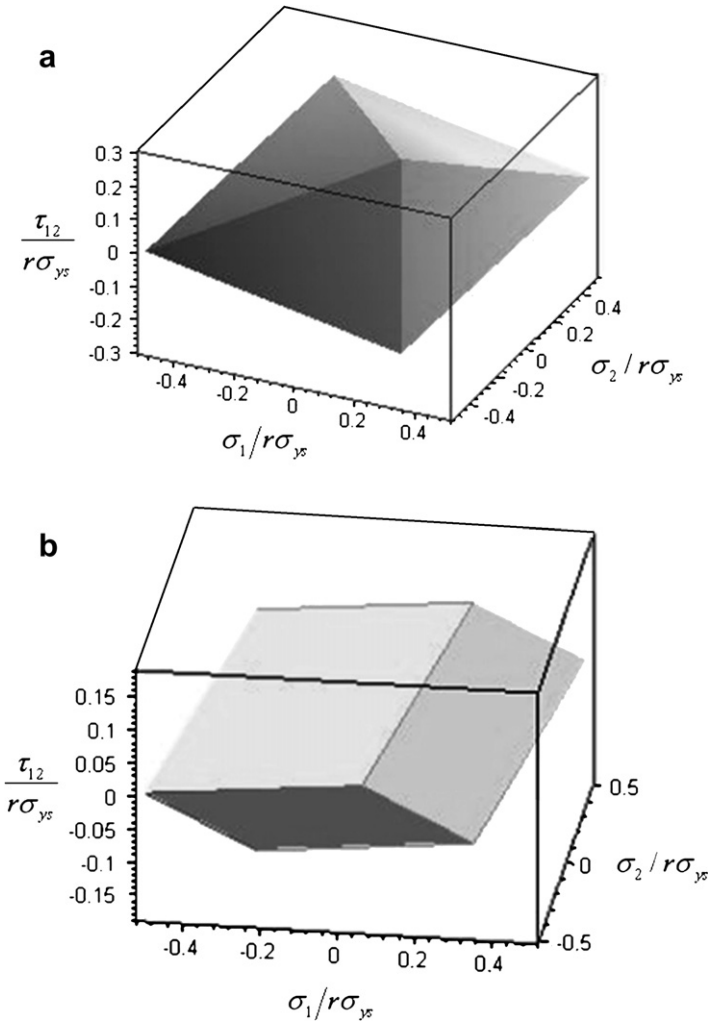

Fig. 7. The initial yield surfaces of (a) the SI-square cell and (b) the N-Kagome cell.

5.2. Buckling surface

Still consider the applied stress state shown in Figs. 3c and 4b, and the unit cell is assumed to buckle if any strut inside the cell buckles. According to the results of Timoshenko and Gere (1961), the buckling load, T_{cr}, for one strut within the unit cell is given by $T_{cr} = \frac{n^2\pi^2 E_s I}{l^2}$, where I is the moment of inertia ($I = bt^3/12$), and n is the end constraint factor which depends on the degree of constraint to rotation at the end nodes. The cells of the lattice materials may buckle in many different modes and it is complicated to analyze them completely for each lattice. For the stretching-dominated structures, we make such an approximation that the buckling mode of the periodic lattice is near to that of the fixed–fixed boundary conditions ($n = 2$). Based on the approximation of taking $n = 2$, the calculation of buckling loads corresponds to the upper bounds to the buckling strengths. To simplify the problem, the fixed–fixed boundary conditions ($n = 2$) are assumed for predictions of the buckling loads of all the stretching-dominated lattices in this paper. For the triangular lattice, the predictions of buckling loads by taking $n = 2$ are very close to the precise results. But for the Kagome lattice, the predictions of buckling loads by taking $n = 2$ are not as accurate as that of the triangular lattice (Hutchinson et al., 2003). Thus, the buckling conditions for each strut are given by,

$$N_i = -T^i_{cr}, \quad i = 1 \ldots 4, \tag{27}$$

where the internal force, N_i, is given by Eqs. (20) and (21), and T^i_{cr} is the buckling load of ith strut, that is, $T^1_{cr} = T^4_{cr} = \frac{1}{3}\pi^2 E_s b \frac{t^3}{l^2}$ and $T^2_{cr} = T^3_{cr} = \frac{2}{3}\pi^2 E_s b \frac{t^3}{l^2}$ for the SI-square cell, and $T^1_{cr} = T^2_{cr} = T^3_{cr} = \frac{1}{3}\pi^2 E_s b \frac{t^3}{l^2}$ and $T^4_{cr} = \pi^2 E_s b \frac{t^3}{l^2}$ for the N-Kagome cell.

The buckling surface equation of the unit cell corresponds to the buckling equation of the first buckling strut. Therefore, the buckling equation can be given by

$$\min(N_i + T^i_{cr}) = 0, \quad i = 1 \ldots 4. \tag{28}$$

The full expressions of the buckling surface equations of the two cells are given by

$$\min \left\{ \begin{array}{l} \frac{2-\sqrt{2}}{2}(\sigma_1+\sigma_2) - \tau_{12} + \frac{\pi^2 E_s}{3}\left(\frac{t}{l}\right)^3, \frac{-(\sqrt{2}-1)\sigma_1}{2} + \frac{\sigma_2}{2} + \frac{\pi^2 E_s}{3}\left(\frac{t}{l}\right)^3 \\ \frac{\sigma_1}{2} - \frac{(\sqrt{2}-1)\sigma_2}{2} + \frac{\pi^2 E_s}{3}\left(\frac{t}{l}\right)^3, \frac{2-\sqrt{2}}{2}(\sigma_1+\sigma_2) + \tau_{12} + \frac{\pi^2 E_s}{3}\left(\frac{t}{l}\right)^3 \end{array} \right\} = 0 \quad \text{(SI-square)}, \tag{29}$$

$$\min \left\{ \begin{array}{l} -\frac{3-\sqrt{3}}{6}\sigma_1 + \frac{5\sqrt{3}-3}{6}\sigma_2 - 2\tau_{12} + \frac{\pi^2 E_s}{3}\left(\frac{t}{l}\right)^3, \\ -\frac{3-\sqrt{3}}{6}\sigma_1 + \frac{5\sqrt{3}-3}{6}\sigma_2 + 2\tau_{12} + \frac{\pi^2 E_s}{3}\left(\frac{t}{l}\right)^3, \\ \frac{7\sqrt{3}-3}{6}\sigma_1 - \frac{3+\sqrt{3}}{6}\sigma_2 + \frac{\pi^2 E_s}{3}\left(\frac{t}{l}\right)^3, \frac{\sqrt{3}-1}{6}(\sigma_1+\sigma_2) + \frac{\pi^2 E_s}{3}\left(\frac{t}{l}\right)^3 \end{array} \right\} = 0 \quad \text{(N-Kagome)}. \tag{30}$$

5.3. Collapse analysis

The collapse analysis is performed considering both the effect of buckling and initial yielding in the condition of in-plane stress state, and the tensional and compressive yield strength are assumed to be the same. At low relative densities the honeycomb tends to collapse due to buckling. As the relative density increases, the collapse mode gradually changes to plastic yielding. Figs. 8 and 9 show the collapse surfaces of the SI-square cell and N-Kagome cell under different kinds of applied stresses, with the material constants $\sigma_{ys}/E_s = 10^{-3}$ and the relative density $r = 0.05$ and 0.025. Since the collapse analyses of the two cells are similar, only the SI-square cell is taken for detailed discussion.

Fig. 8a shows the collapse surface of the SI-square cell in the stress space of σ_1 and σ_2, with the material constants $\sigma_{ys}/E_s = 10^{-3}$ and the relative density $r = 0.05$. In this case the collapse is the combined effect of both buckling and initial yielding. As shown in Fig. 8a the buckling surface is not close since all struts inside the unit cell will be in tension when the proportion of the external applied stresses, σ_1/σ_2, is in a certain range. When the external applied stresses, σ_1 and σ_2, are in the domain between the lines OB and OC, the buckling of the unit cell is earlier than yielding, and thus it collapses due to buckling. When the external applied stresses, σ_1 and σ_2, are in the other domain, the unit cell collapses due to yielding. Therefore, the admissible domain for the external applied stresses, σ_1 and σ_2, is the internal region of $ABCDEA$ as shown in Fig. 8a.

Since the initial yield surface of the SI-square honeycomb possesses the 4-fold rotational symmetry, the yield surface under the stress space of σ_1 and τ_{12} is the same as that under the stress space of σ_2 and τ_{12}, as shown in Fig. 8b. Since there is no contribution of the applied stress τ_{12} to the internal forces in the 2nd and 3rd struts (see Eq. (20)), the buckling curves of the 2nd and 3rd struts are both vertical, for which the buckling surface under the stress space of σ_1 and τ_{12} is closed. The admissible domain is the internal region of $ABCDEFA$ in Fig. 8b.

Keep the material parameter, σ_{ys}/E_s, unchanged and reduce the relative density, r, to 0.025, and then the buckling will be more likely to occur in the honeycomb, as shown in Fig. 8c and d. In the stress space of σ_1 and τ_{12} or σ_2 and τ_{12}, the collapses are governed only by buckling.

As can be seen from Fig. 8b and d, if there exists only the external applied shear stress, τ_{12}, the buckling of this honeycomb will be earlier than yielding, which means the honeycomb collapses due to shear buckling. In fact, the shear buckling also exists in other kinds of planar lattice structures, and it has great influence on collapse at low relative densities. However, to the best of our knowledge, the shear buckling of lattice structures has not been considered in the previous work.

In Fig. 8, the relative densities of the SI-square cells are $r = 0.05$ and $r = 0.025$. It is clear if the relative density of the SI-square cell is bigger than the value of about 0.06, the collapse mode will be yielding only, and the figures are omitted here.

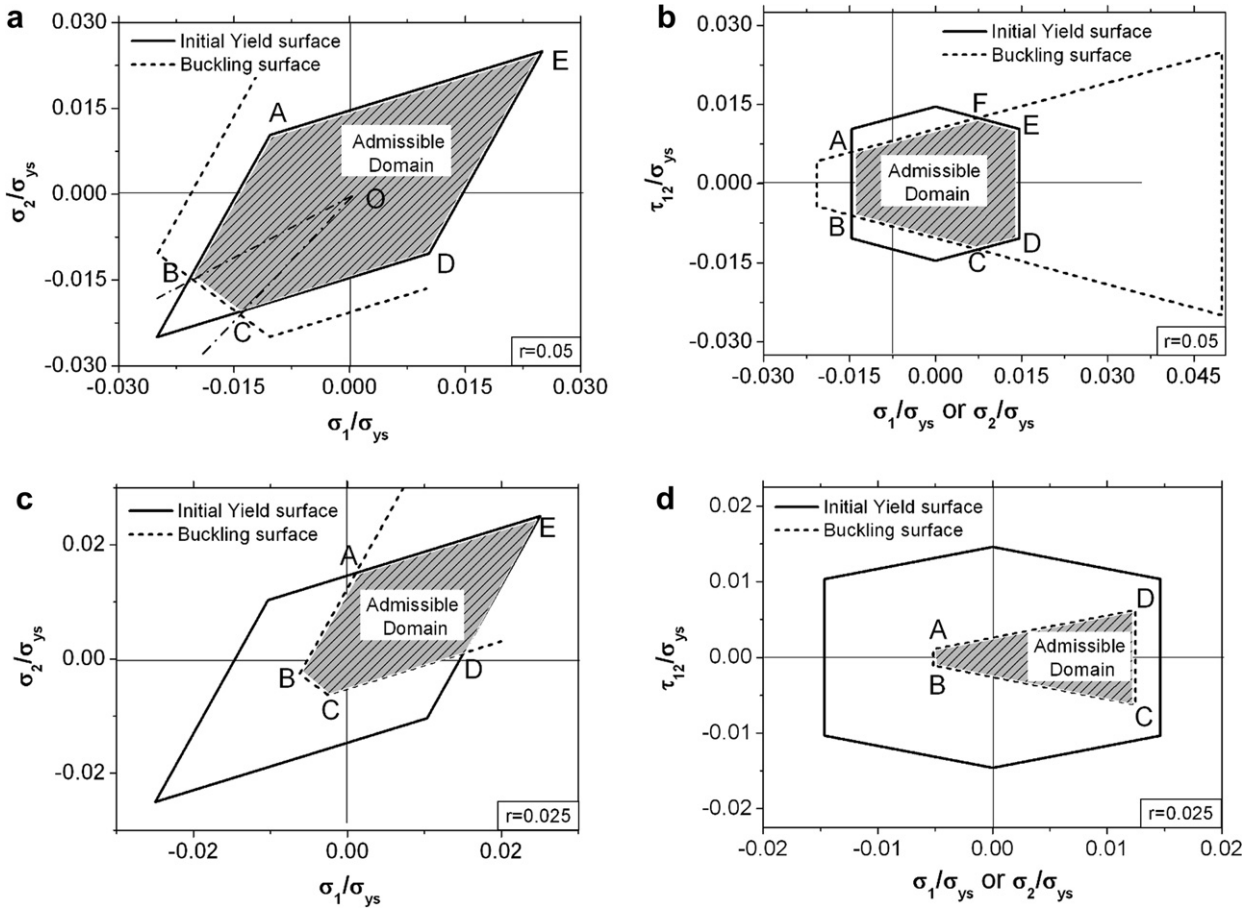

Fig. 8. The collapse surfaces of the SI-square cell in the stress spaces of σ_1, σ_2 and σ_1 or σ_2, τ_{12} ($\sigma_{ys}/E_s = 10^{-3}$, $r = 0.05$ and 0.025).

6. Anisotropy of in-plane mechanical properties of various cells

In order to compare mechanical properties of various cells, the effective elastic modulus, yield strength and elastic buckling strength under in-plane uniaxial loading are calculated. The effective elastic modulus in an arbitrary direction can be obtained by the axis-rotation formulas. Degenerated from the results of the yield surface and buckling surface equations, the uniaxial yielding and buckling strength in an arbitrary direction can also be calculated.

Under uniaxial loading, a critical relative density is defined in order to describe the transform of the collapse mode from buckling to yielding. The uniaxial initial yield strength, $\sigma^*_{pl}(\theta)$, in the θ direction is linearly dependent on the relative density, r, the yield stress of cell material, σ_{ys}, and a function ($f_1(\theta)$) that is only dependent on θ. Therefore, $\sigma^*_{pl}(\theta)$ can be given as follow (Wang and McDowell, 2004, 2005),

$$\sigma^*_{pl}(\theta) = \sigma_{ys} f_1(\theta) r. \tag{31}$$

Similarly, the uniaxial buckling strength, $\sigma^*_e(\theta)$, in the θ direction can be given by

$$\sigma^*_e(\theta) = E_s f_2(\theta) r^3, \tag{32}$$

where $f_2(\theta)$ also is a function only dependent on θ. From Eqs. (31) and (32), the critical relative density, $r_{cr}(\theta)$, can be obtained by making the uniaxial initial yield strength equal to the uniaxial buckling strength, i.e.

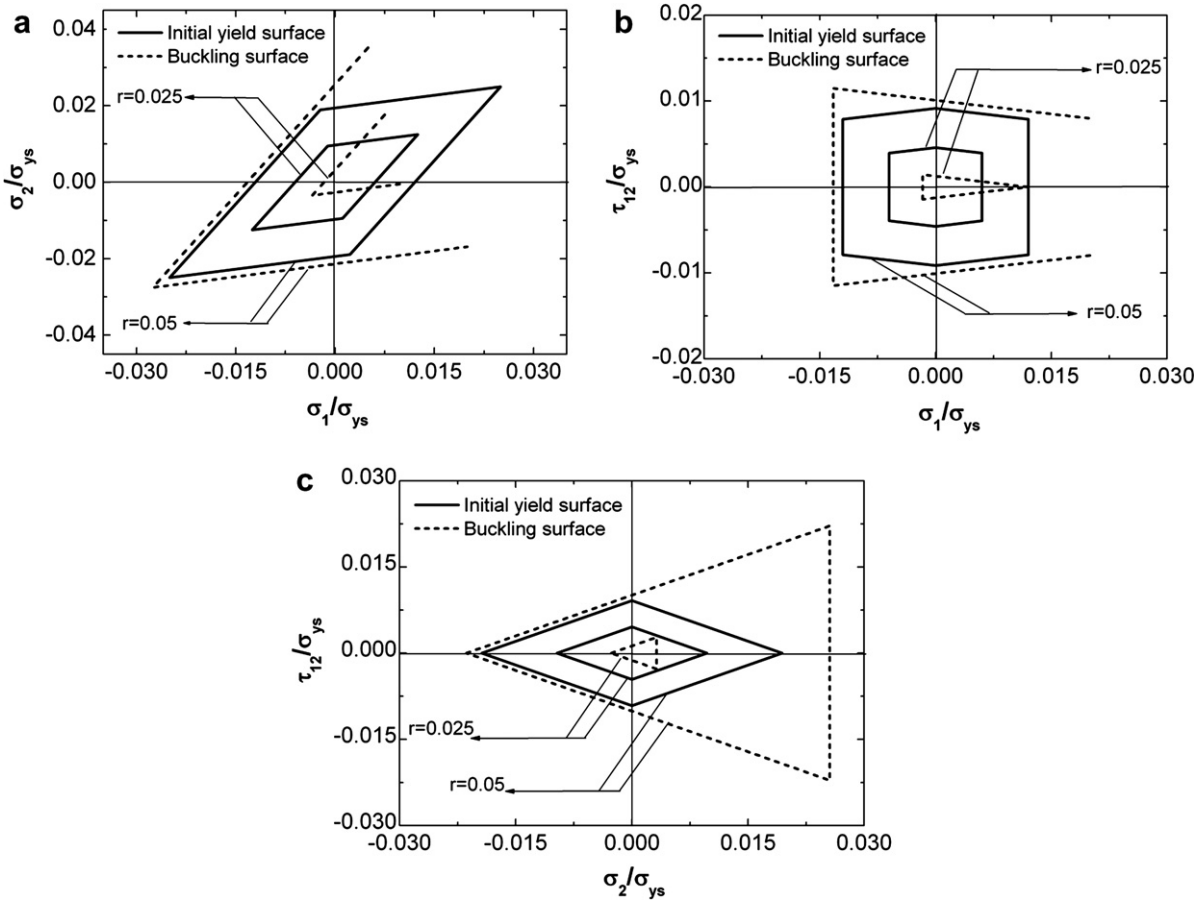

Fig. 9. The collapse surfaces of the N-Kagome cell in the stress spaces of (a) σ_1, σ_2 (b) σ_1, τ_{12} and (c) σ_2, τ_{12} ($\sigma_{ys}/E_s = 10^{-3}$, $r = 0.05$ and 0.025).

$$r_{cr}(\theta) = \sqrt{\frac{\sigma_{ys}}{E_s}\frac{f_1(\theta)}{f_2(\theta)}}. \tag{33}$$

Since the functions, $f_1(\theta)$ and $f_2(\theta)$, are determinate for given lattice structures, the critical relative density is a natural property of the lattice structures. Possessing higher critical relative density means that the buckling collapse is more likely to occur in the unit cell. From Eq. (33), one can find that the critical relative density depends on the loading direction and can be obtained using the results of uniaxial yielding and buckling strength.

6.1. Anisotropy of in-plane mechanical properties of the SI-square cell

The effective elastic modulus of the SI-square cell in the direction of the angle (θ) with the x_1 direction is given by

$$\frac{E^*(\theta)}{E_s} = \frac{2-\sqrt{2}}{2}\frac{1}{1-2\left(\sqrt{2}-1\right)\sin^2\theta\cos^2\theta}r, \quad \left(0 \leqslant \theta \leqslant \frac{\pi}{4}\right). \tag{34}$$

Due to the 4-fold rotational symmetry of the unit cell, only the expression in the range of $0 \leqslant \theta \leqslant \frac{\pi}{4}$ is given. Therefore, the maximum and minimum effective moduli are,

$$\frac{E^*_{\max}}{E_s} = 0.369r, \quad \theta = \pm\frac{\pi}{4}, \pm\frac{3\pi}{4}, \tag{35}$$

$$\frac{E^*_{\min}}{E_s} = \frac{E^*_1}{E_s} = \frac{E^*_2}{E_s} = 0.293r, \quad \theta = \pm\frac{\pi}{2}, 0, \pi. \tag{36}$$

Since the problem of the unit cell under the uniaxial applied tensional stress, σ, in the θ direction is equivalent to that under the applied stresses, $\sigma_1 = \sigma\cos^2\theta$, $\sigma_2 = \sigma\ \sin^2\theta$ and $\tau_{12} = \sigma\sin\theta\cos\theta$, the uniaxial initial yielding strength, $\sigma^*_{pl}(\theta)$, in the θ direction can be calculated using the initial yield surface equation, Eq. (23), i.e.

$$\frac{\sigma^*_{pl}(\theta)}{\sigma_{ys}} = \begin{cases} \frac{1}{(1+\sqrt{2})(\sqrt{2}-2\sin^2\theta)}r, & (0 \leqslant \theta \leqslant 0.152\pi) \\ \frac{1}{(1+\sqrt{2})(\sqrt{2}+\sqrt{2}\sin\theta\cos\theta-1)}r, & \left(0.152\pi \leqslant \theta \leqslant \frac{\pi}{4}\right) \end{cases}. \tag{37}$$

From the above equations, we can get the initial yield strength in the principal directions,

$$\frac{\sigma^*_{pl1}}{\sigma_{ys}} = \frac{\sigma^*_{pl2}}{\sigma_{ys}} = 0.293r, \quad \frac{\sigma^*_{\text{diagpl}}}{\sigma_{ys}} = 0.369r, \tag{38}$$

where σ^*_{diagpl} is the initial yield strength in the diagonal directions. The values of the maximum and minimum uniaxial initial yielding strength are,

$$\frac{\sigma^*_{pl\max}}{\sigma_{ys}} = 0.418r, \quad \left(\theta = \frac{n\pi}{2} \pm 0.152\pi,\ n = 1\ldots4\right), \tag{39}$$

$$\frac{\sigma^*_{pl\min}}{\sigma_{ys}} = 0.293r, \quad \left(\theta = \frac{n\pi}{2},\ n = 1\ldots4\right). \tag{40}$$

Similarly, the uniaxial buckling strength, $\sigma^*_e(\theta)$, in the θ direction can be obtained as follow,

$$\frac{\sigma^*_e(\theta)}{E_s} = \begin{cases} \frac{2\sqrt{2}}{3}\frac{\pi^2}{(2+\sqrt{2})^3(\sqrt{2}-2\sin^2\theta)}r^3, & (0 \leqslant \theta \leqslant 0.0596\pi), \\ \frac{\sqrt{2}}{3}\frac{\pi^2}{(2+\sqrt{2})^3(\sqrt{2}\sin\theta\cos\theta+\sqrt{2}-1)}r^3, & \left(0.0596\pi \leqslant \theta \leqslant \frac{\pi}{4}\right). \end{cases} \tag{41}$$

The buckling strength in the principal directions are,

$$\frac{\sigma^*_{e1}}{E_s} = \frac{\sigma^*_{e2}}{E_s} = 0.165r^3, \quad \frac{\sigma^*_{\text{diage}}}{E_s} = 0.104r^3, \tag{42}$$

where σ^*_{e1}, σ^*_{e2} and σ^*_{diagpl} are the buckling strength in the x_1, x_2 and diagonal directions, respectively. The values of the maximum and minimum uniaxial buckling strength are,

$$\frac{\sigma^*_{e\max}}{E_s} = 0.174r^3, \quad \left(\theta = \frac{n\pi}{2} \pm 0.0596\pi,\ n = 1\ldots4\right), \tag{43}$$

$$\frac{\sigma^*_{e\min}}{E_s} = 0.104r^3, \quad \left(\theta = \frac{n\pi}{2} - \frac{\pi}{4},\ n = 1\ldots4\right). \tag{44}$$

6.2. Anisotropy of in-plane mechanical properties of the N-Kagome cell

Since the N-Kagome cell is transversely isotropic, the effective elastic modulus $E^*(\theta)$ in the θ direction is always equal to $0.241rE_s$.

The uniaxial initial yielding strength, $\sigma^*_{pl}(\theta)$, in the θ direction can be calculated using the initial yield surface equation, Eq. (24), i.e.

$$\frac{\sigma^*_{pl}(\theta)}{\sigma_{ys}} = \frac{6+4\sqrt{3}}{(1+\sqrt{3})\left[(16+8\sqrt{3})\cos^2\theta - 5 - 3\sqrt{3}\right]}r, \quad \left(0 \leqslant \theta \leqslant \frac{\pi}{6}\right). \tag{45}$$

From the above equations, the initial uniaxial initial strength in the x_1, x_2 directions are,

$$\frac{\sigma^*_{pl1}}{\sigma_{ys}} = 0.241r, \quad \frac{\sigma^*_{pl2}}{\sigma_{ys}} = 0.388r. \tag{46}$$

Similarly, the uniaxial buckling strength, $\sigma^*_e(\theta)$, in the θ direction can be obtained as follows

$$\frac{\sigma^*_e(\theta)}{E_s} = \frac{\pi^2}{\left(3+\sqrt{3}\right)\left[8\left(2+\sqrt{3}\right)\cos^2\theta - 5 - 3\sqrt{3}\right]} r^3, \quad \left(0 \leqslant \theta \leqslant \frac{\pi}{6}\right). \tag{47}$$

The uniaxial buckling strength in the x_1, x_2 directions are given by,

$$\frac{\sigma^*_{e1}}{E_s} = \frac{\sigma^*_{e\min}}{E_s} = 0.106r^3, \quad \frac{\sigma^*_{e2}}{E_s} = \frac{\sigma^*_{e\max}}{E_s} = 0.171r^3. \tag{48}$$

6.3. Comparison of in-plane mechanical properties for six lattice cells

The effective elastic moduli, initial yielding strength, buckling strength, and critical relative density under uniaxial loading in arbitrary directions of five cell patterns, including the triangular, Kagome, mixed, SI-square and N-Kagome cells, are calculated. The full expressions of mechanical properties of three cells are listed in Appendix. Besides, the values or scopes of mechanical properties for these 2D lattice structures are listed in Table 1 for comparison.

According to Eqs. (35) and (36), the average of the maximum and minimum effective moduli of the SI-square cell is equal to the effective modulus of the Kagome cell, which indicates that the average stiffness of these four cells are equally high. Among these lattice cells, the Kagome lattice possesses much higher stability. In Fig. 10c, the normalized buckling strength of the Kagome cell is more than twice that of the other cells. From Fig. 10d, one can find that the critical relative density of the Kagome cell is very low, which means the failure of the Kagome cell will be yielding collapse at lower relative density. For the triangular and mixed cells, the uniaxial admissible applied stresses will be much lower when the relative densities are lower than 0.05, compared with the other two cells.

Due to slight difference in configuration, the effective modulus and yield strength are different for the mixed cell and the SI-square cell. Note that the difference only exists in the cavity directions. If one cell is rotated an angle of $\pi/4$, the effective modulus and yield strength of these two cells will be exactly the same. However, it should be noted that the stability of the SI-square cell is about twice than that of the mixed cell. It can be seen from Table 1 that compared with the Kagome cell, the stiffness of the SI-square cell is as high as that of the Kagome cell, and the initial yield strength of the SI-square cell is a little low. However, different from the Kagome cell, the SI-square cell is still able to sustain further load after initial yielding, and the utmost yield strength of the SI-square cell is calculated and found to be higher than the initial yield strength of the Kagome cell. Therefore, the SI-square honeycomb is an excellent structure in load carrying.

Compared with the Kagome cell, the effective stiffness, yield strength and buckling strength of the N-Kagome cell are slightly lower. However, compared with the other existing stretching-dominated 2D lattice structures (triangular, Kagome, diamond, mixed and SI-square cells), the N-Kagome cell possesses the largest

Table 1
Comparison of mechanical properties for various 2D lattice structures

Unit cell	Triangular	Kagome	Mixed	SI-square	N-Kagome
$E^*/(rE_s)$	0.333	0.333	0.293–0.369	0.293–0.369	0.241
$G^*_{12}/(rE_s)$	0.125	0.125	0.104	0.147	0.079
$\sigma^*_e/(r^3E_s)$	0.091–0.137	0.366–0.548	0.041–0.105	0.104–0.174	0.106–0.171
$\sigma^*_{pl}/(r\sigma_{ys})$	0.333–0.5	0.333–0.5	0.293–0.418	0.293–0.418	0.241–0.388
$\tau^*_{pl12}/(r\sigma_{ys})$	0.289	0.289	0.207	0.293	0.183
$\Omega r^2/l^2$	$3\sqrt{3}$	$6\sqrt{3}$	$3+2\sqrt{2}$	$2\left(3+2\sqrt{2}\right)$	$4\left(3+2\sqrt{3}\right)$

Note: Ω denotes the area of the largest continuous cavity of lattice structure.

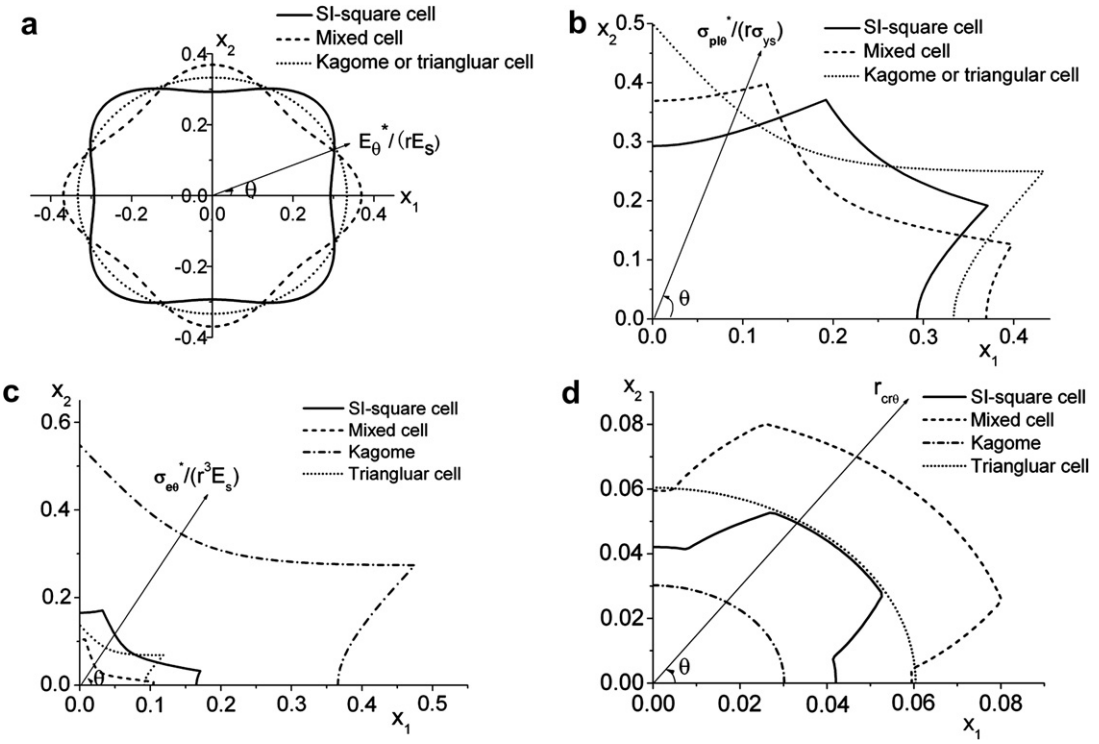

Fig. 10. Normalized properties of (a) elastic modulus, (b) yield strength, (c) buckling strength and (d) critical relative density of four cells under uniaxial loading ($\sigma_{ys}/E_s = 10^{-3}$).

continuous cavities at fixed relative densities and wall thicknesses. Its area is twice than that of the other lattice structures (see Table 1). Therefore, the N-Kagome lattice structure is convenient for oil storage, disposal of heat exchanger, battery deploying and for other functions.

7. Conclusions

Based on the considerations to enhance the stability and other properties of the mixed cell and the Kagome cell, two novel 2D lattice materials noted as SI-square cell and N-Kagome cell are designed in this paper. Their mechanical properties are investigated by analytical methods, including stiffness, yield surface, buckling surface and collapse mechanisms. The analytical effective stiffness is verified by means of FE simulations. Some conclusions related to their mechanical properties can be drawn as follows:

(1) The collapse analysis indicates that the elastic buckling of lattice structures under macroscopic shear loading, which have not been considered before, will have prominent influence, especially at low relative densities. The critical relative density, defined under uniaxial loading, is a natural property of the lattice structures.
(2) For the SI-square honeycomb, both the bulk modulus, k^*, and the combination of shear modulus, G_e, are relatively close to the corresponding optimal values.
(3) It is found that the proposed SI-square cell has similar high stiffness and strength as those of the mixed cell while its buckling resistance is about twice that of the mixed cell, which indicates that the SI-square honeycomb is an excellent structure in load carrying.
(4) The yield strength of the N-Kagome cell is slightly lower than the Kagome cell in all directions. But compared with the other existing stretching-dominated 2D lattice structures, the N-Kagome cell possess the largest continuous cavities at fixed relative densities and wall thicknesses, with an area that is twice than that of the other lattice structures, which is convenient for oil storage, disposal of heat exchanger, battery deploying and for other functions.

The two planar lattice materials proposed in this paper both possess special mechanical properties, which provide some available choices in lightweight structure design.

Acknowledgements

The authors are grateful for the support by National Natural Science Foundation of China under Grants #90305015, #10502027 and #10328203. Supported by the Special Funds for the Major State Basic Research Projects of China (#G2003CB615603, #G2006CB601202) is also acknowledged.

Appendix A. Effective material properties of three repetitive cells under uniaxial loading

The mixed cell:

$$\frac{E^*(\theta)}{E_s} = \frac{2\sqrt{2}+2}{6+5\sqrt{2}+4\left(\sqrt{2}+2\right)\sin^2\theta\cos^2\theta} r, \quad \left(0 \leqslant \theta \leqslant \frac{\pi}{4}\right). \tag{A.1}$$

$$\frac{\sigma^*_{pl}(\theta)}{\sigma_{ys}} = \begin{cases} \frac{1}{\left(1+\sqrt{2}/2\right)\cos 2\theta+1} r, & (0 \leqslant \theta \leqslant 0.098\pi), \\ \frac{1}{\left(1+\sqrt{2}\right)\left[\sqrt{2}-2\cos^2(\theta+\pi/4)\right]} r, & \left(0.098\pi \leqslant \theta \leqslant \frac{\pi}{4}\right). \end{cases} \tag{A.2}$$

$$\frac{\sigma^*_e(\theta)}{E_s} = \begin{cases} \frac{\sqrt{2}}{3} \frac{\pi^2}{\left(2+\sqrt{2}\right)^2\left[2\left(1+\sqrt{2}\right)\cos^2\theta-1\right]} r^3, & (0 \leqslant \theta \leqslant 0.0228\pi), \\ \frac{1}{6} \frac{\pi^2}{\left(2+\sqrt{2}\right)^2\left[2\left(1+\sqrt{2}\right)\sin\theta\cos\theta+1\right]} r^3, & \left(0.0228\pi \leqslant \theta \leqslant \frac{\pi}{4}\right). \end{cases} \tag{A.3}$$

The Kagome cell:

$$\frac{E^*(\theta)}{E_s} = \frac{1}{3} r. \tag{A.4}$$

$$\frac{\sigma^*_e(\theta)}{E_s} = \frac{1}{9} \frac{\pi^2}{4\cos^2\theta - 1} r^3, \quad \left(0 \leqslant \theta \leqslant \frac{\pi}{6}\right). \tag{A.5}$$

The triangular cell:

$$\frac{E^*(\theta)}{E_s} = \frac{1}{3} r. \tag{A.6}$$

$$\frac{\sigma^*_{pl}(\theta)}{\sigma_{ys}} = \frac{r}{4\cos^2\theta - 1}, \quad \left(0 \leqslant \theta \leqslant \frac{\pi}{6}\right). \tag{A.7}$$

$$\frac{\sigma^*_e(\theta)}{E_s} = \frac{1}{36} \frac{\pi^2}{4\cos^2\theta - 1} r^3, \quad \left(0 \leqslant \theta \leqslant \frac{\pi}{6}\right). \tag{A.8}$$

References

Andrews, E.W., Gioux, G., Onck, P., Gibson, L.J., 2001. Size effects in ductile cellular solids. Part II: experimental results. International Journal of Mechanical Sciences 43, 701–713.

Ashby, M.F., 2000. Multi-objective optimization in material design and selection. Acta Materialia 48, 359–369.

Ashby, M.F., Evans, A.G., Fleck, N.A., Gibson, L.J., Hutchinson, J.W., Wadley, H.N.G., 2000. Metal Foams: A Design Guide. Butterworth Heinemann, Boston.

Cochran, J., Lee, K.J., McDowell, D.L., Sanders, T., Church, B., Clark, J., Dempsey, B., Hayes, A., Hurysz, K., McCoy, T., Nadler, J., Oh, R., Seay, W., Shapiro, B., 2000. Low density monolithic metal honeycombs by thermal chemical processing. In: Fourth Conference on Aerospace Materials, Processes and Environmental Technology, Huntsville, Alabama, September 18–20.

Evans, A.G., 2001. Lightweight materials and structures. Materials Research Bulletin 26, 790–797.

Evans, A.G., Hutchinson, J.W., Fleck, N.A., Ashby, M.F., Wadley, H.N.G., 2001. The topological design of multifunctional cellular metals. Progress in Materials Science 46, 309–327.

Francfort, G.A., Murat, F., 1986. Homogenization and optimal bounds in linear elasticity. Archive for Rational Mechanics and Analysis 94, 307–334.

Gere, J.M., Timoshenko, S.P., 1984. Mechanics of Materials, second ed. Wadsworth Inc.
Gibson, L.J., Ashby, M.F., 1997. Cellular Solids: Structure and properties, second ed. Cambridge University Press, Cambridge.
Hashin, Z., 1965. On elastic behaviour of fibre reinforced materials of arbitrary transverse phase geometry. Journal of the Mechanics and Physics of Solids 13, 119–134.
Hashin, Z., Shtrikman, S., 1963. A variational approach to the theory of the elastic behaviour of multiphase materials. Journal of the Mechanics and Physics of Solids 11, 127–140.
Hutchinson, R.G., Wicks, N., Evans, A.G., Fleck, N.A., Hutchinson, J.W., 2003. Kagome plate structures for actuation. International Journal of Solids and Structures 40, 6969–6980.
Hyun, S., Torquato, S., 2000. Effective elastic and transport properties of regular honeycombs for all densities. Journal of Materials Research 15, 1985–1993.
Kantor, Y., Bergman, D.J., 1984. Improved rigorous bounds on the effective elastic moduli of a composite material. Journal of the Mechanics and Physics of Solids 32, 41–62.
Kim, T., Hodson, H.P., Lu, T.J., 2004. Fluid-flow and end wall heat-transfer characteristics of an ultralight lattice-frame material. International Journal of Heat and Mass Transfer 47, 1129–1140.
Kim, T., Hodson, H.P., Lu, T.J., 2005. Contribution of vortex structures and flow separation to local and overall pressure and heat transfer characteristics in an ultralightweight lattice material. International Journal of Heat and Mass Transfer 48, 4243–4264.
Liu, J.S., Lu, T.J., 2004. Multi-objective and multi-loading optimization of ultralightweight truss materials. International Journal of Solids and Structures 41, 619–635.
Lu, T.J., Valdevit, L., Evans, A.G., 2005. Active cooling by metallic sandwich structures with periodic cores. Progress in Materials Science 50, 789–815.
Milton, G.W., Kohn, R.V., 1988. Variational bounds on the effective moduli of anisotropic composites. Journal of the Mechanics and Physics of Solids 36, 597–629.
Onck, P.R., Andrews, E.W., Gibson, L.J., 2001. Size effects in ductile cellular solids, Part I: modeling. International Journal of Mechanical Sciences 43, 681–699.
Papka, S.D., Kyriakides, S., 1998. Experiments and full-scale numerical simulations of in-plane crushing of a honeycomb. Acta Materialia 46 (8), 2765–2776.
Smith, H.B., Hutchinson, J.W., Evans, A.G., 2001. Measurement and analysis of the structural performance of cellular mental sandwich construction. International Journal of Mechanical Sciences 43, 1945–1963.
Timoshenko, S.P., Gere, J.M., 1961. Theory of Elastic Stability, second ed. McGraw-Hill, New York.
Wang, A.J., McDowell, D.L., 2003. Effect of defects on in-plane properties of periodic metal honeycombs. International Journal of Mechanical Sciences 43, 1799–1813.
Wang, A.J., McDowell, D.L., 2004. In-plane stiffness and yield strength of periodic metal honeycombs. ASME Journal of Engineering Materials and Technology 126, 137–156.
Wang, A.J., McDowell, D.L., 2005. Yield surfaces of various periodic metal honeycombs at intermediate relative density. International Journal of Plasticity 21, 285–320.
Wicks, N., Hutchinson, J.W., 2001. Optimal truss plates. International Journal of Solids and Structures 38, 5165–5183.
Zhang, J., Ashby, M.F., 1992. Buckling of honeycombs under in-plane biaxial stresses. International Journal of Mechanical Sciences 34 (6), 491–509.